Available online at www.sciencedirect.com
SCIENCE DIRECT
Polymer 46 (2005) 11786–11797
polymer
www.elsevier.com/locate/polymer

Non-linear, rate-dependent strain-hardening behavior of polymer glasses

Michael Wendlandt, Theo A. Tervoort*, Ulrich W. Suter

ETH Zurich, Department of Materials, Zürich CH-8093, Switzerland

Received 9 June 2005; received in revised form 22 August 2005; accepted 25 August 2005
Available online 14 October 2005

Abstract

This study is concerned with the finite, large strain deformation behavior of polymeric glasses. True stress–strain curves in uniaxial compression obtained for five different polymeric glasses: polycarbonate, polystyrene, poly(2,6-dimethyl-1,4-phenylene oxide), and linear and cross-linked poly(methylmethacrylate), revealed a strain-hardening response during plastic deformation that is strain-rate dependent and deviates from neo-Hookean behavior. An empirical modification of the so-called compressible Leonov model by a strain dependent activation volume is suggested, which describes the strain-rate dependent large strain behavior of these glassy polymers in good agreement with experimental data.

Keywords: Polymer glasses; Strain-hardening; Activation volume

1. Introduction

An important aspect of the mechanical behavior of polymers is the strain-hardening response during large-strain plastic deformation. It is now generally accepted that the long-chain nature of polymers in general, and polymer glasses especially, plays an important role in their mechanical response at large deformations. During plastic deformation, the covalent chains orient, resulting in anisotropic materials with enhanced properties in the drawing direction. The exact nature of this orientation process, however, has not yet been resolved, which hampers the development of efficient constitutive relations and, ultimately, the design of new polymeric materials with tailored mechanical properties.

A typical stress–strain curve in uniaxial compression of an amorphous polymer deformed at five different strain rates (far) below its glass transition is shown in Fig. 1. The temperature and strain-rate dependent yield stress of glassy polymers is adequately described by the Eyring model [1], in which the so-called activation volume determines the decrease of activation energy for segmental motion in the direction of the applied stress. At large strains in the post-yield regime, amorphous polymers typically reveal a drop in the true stress with increasing plastic strain, usually referred to as intrinsic strain-softening. The exact physical origin of strain-softening has not been elucidated yet, but appears to be related to the process of physical aging [2,3]. Physical aging, the slow approach towards thermodynamic equilibrium, tends to increase the yield stress as a function of aging time. This increase is reversed by plastic deformation, which is the above-mentioned strain-softening response, also called 'mechanical rejuvenation' [4,5]. After strain-softening, the stress increases again with increasing plastic strain. The latter characteristic feature of stress–strain curves of polymeric glasses, which is the main focus of this study, is called strain-hardening and is usually described by a rubber-elastic response of an underlying entanglement network with strain-hardening modulus G_R (note that we use this nomenclature for the strain hardening modulus as suggested by van Melick et al. [6]).

Haward and Thackray [7] were the first to incorporate concepts of rubber-elasticity into the constitutive modeling of polymer glasses to account for strain-hardening. They assumed that the total stress can be decoupled into a viscoelastic part, evolving from segmental motions, and a rubber-elastic part with a given finite extensibility, evolving from the rubber-elastic response of an entanglement network active in the polymeric solid during plastic deformation. This one-dimensional model was extended by Boyce et al. [8] into a three-dimensional finite strain formulation, the so-called 'BPA-model'. Later, it was shown by Haward [9,10] that stabilization of deformation zones during plastic deformation could also be realized with simple neo-Hookean strain-hardening behavior. Neo-Hookean strain hardening behavior was also observed experimentally in uniaxial tension for a number of linear glassy and semi-crystalline polymers [10,11]. In a recent study [6]

* Corresponding author.
E-mail address: theo.tervoort@mat.ethz.ch (T.A. Tervoort).

0032-3861/$ - see front matter © 2005 Elsevier Ltd. All rights reserved.
doi:10.1016/j.polymer.2005.08.079

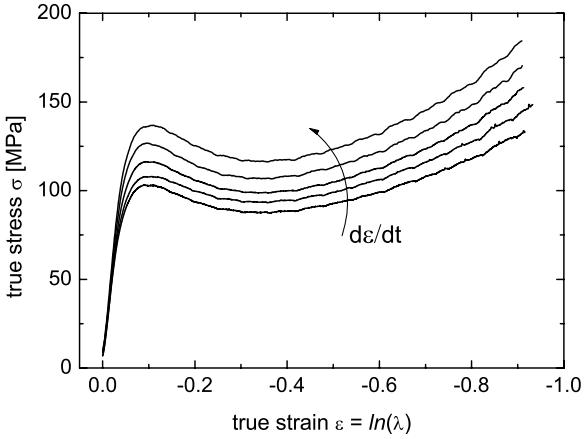

Fig. 1. Typical stress–strain curves of a polymeric glass obtained in uniaxial compression at different strain rates $\dot{\varepsilon}$.

neo-Hookean strain-hardening was found for a series of poly(styrene)-poly(phenyleneoxide) blends and even for cross-linked poly(styrene). In all cases, the strain-hardening increased with increasing entanglement or cross-link density. In other studies, neo-Hookean strain-hardening was found to play an important role in the stabilization of localized deformation zones [12–14]. The object of this paper is to investigate in more detail the contribution of the entanglement network and segmental motion to the total strain-hardening response of a number of linear and cross-linked polymer glasses. Especially, the effect of a non-constant activation volume on the total stress–strain behavior will be discussed.

2. Theory

2.1. The compressible Leonov model

The theoretical analysis of the deformation behavior of polymer glasses in this study is based on a modification of the compressible Leonov model [4,15]. First, a brief description of a standard single Leonov mode will be presented, while the extension to a non-constant activation volume will be discussed in more detail in Section 5. The standard three-dimensional Leonov model provides a constitutive description of the finite strain, non-linear viscoelastic behavior of polymeric glasses. In this model, the total Cauchy stress $\mathbf{T}$ is decomposed in a driving stress $\mathbf{S}$ due to segmental motion and a deviatoric hardening stress $\mathbf{R}$ related to an elastic network response:

$$\mathbf{T} = \mathbf{S} + \mathbf{R} \tag{1}$$

The deviatoric hardening stress $\mathbf{R}$ is described by a simple neo-Hookean relation [7,11]:

$$\mathbf{R} = G_R \tilde{\mathbf{B}}^d \tag{2}$$

where $\tilde{\mathbf{B}}$ is the isochoric left Cauchy–Green deformation tensor, G_R is the strain-hardening modulus, and the superscript 'd' denotes the deviatoric part of a tensor.

The driving stress $\mathbf{S}$ consists of a hydrostatic part that is coupled to the relative volume deformation $J = dV/dV_0$, and a deviatoric part, that is determined by the isochoric elastic strain $\tilde{\mathbf{B}}_e$ and can be written as:

$$\mathbf{S} = K(J-1)\mathbf{I} + G\tilde{\mathbf{B}}_e^d \tag{3}$$

where K is the bulk modulus and G the shear modulus. Assuming that the volume deformation remains elastic, the evolution equation for J follows from kinematics: $\dot{J} = J\,\mathrm{tr}(\mathbf{D})\mathbf{I}$, where $\mathbf{D}$ is the strain-rate tensor and the dot denotes the time derivative. The evolution equation for $\tilde{\mathbf{B}}_e$ describes the accumulation of elastic strain (at constant volume) that is reduced because of a plastic strain rate $\mathbf{D}_p$:

$$\mathring{\tilde{\mathbf{B}}}_e = (\mathbf{D}^d - \mathbf{D}_p)\cdot\tilde{\mathbf{B}}_e + \tilde{\mathbf{B}}_e\cdot(\mathbf{D}^d - \mathbf{D}_p) \tag{4}$$

where $\mathring{\tilde{\mathbf{B}}}_e$ is the Jaumann or corotational derivative of $\tilde{\mathbf{B}}_e$. Eyring's molecular rate theory [16–18] forms the basis for the modeling of the plastic strain rate in the present research. It is assumed, that a structural element on an atomistic or molecular scale, e.g. a chain, a side chain, or statistical Kuhn segment in polymers, takes part in an event leading to plastic deformation of a polymer glass by passage over an energy barrier, a so-called 'plastic event'. The jump probability is increased when external work, e.g. stress, aids the passage over the barrier. The Eyring theory leads to a generalized non-Newtonian flow rule that can be used to relate the plastic strain rate to the deviatoric driving stress using a stress-dependent Eyring viscosity η:

$$\mathbf{D}_p = \frac{\mathbf{S}^d}{2\eta(\tau_{eq})} \quad \text{with} \quad \eta(\tau_{eq}) = A\tau_0 \frac{\tau_{eq}/\tau_0}{\sinh(\tau_{eq}/\tau_0)} \tag{5}$$

$$\tau_{eq} = \sqrt{\frac{1}{2}\mathrm{tr}(\mathbf{S}^d\cdot\mathbf{S}^d)} \tag{6}$$

$$\dot{\gamma}_{eq} = \sqrt{2\mathrm{tr}(\mathbf{D}_p\cdot\mathbf{D}_p)} \tag{7}$$

Here, the equivalent stress τ_{eq} is proportional to the von Mises stress, $\dot{\gamma}_{eq}$ is the equivalent plastic strain-rate that reduces to the plastic shear rate for shear flow, and τ_0 describes a characteristic stress:

$$\tau_0 = \frac{kT}{V^*} \tag{8}$$

where V^* is the so-called 'activation volume', which is assigned to a 'plastic event' as described above and treated as a material constant in the Eyring theory. Finally, A is a characteristic time given by

$$A = A_0 \exp\left(\frac{\Delta H_0}{kT}\right) \tag{9}$$

where k is the Boltzmann constant, A_0 constant pre-exponential factor involving the fundamental vibration energy, T the absolute temperature, and ΔH_0 represents the height of the energy barrier at zero equivalent stress. Hence, according to Eqs. (5)–(7), in the Eyring model the equivalent strain rate $\dot{\gamma}_{eq}$

is related to the equivalent stress τ_{eq} as:

$$\dot{\gamma}_{eq} = \frac{1}{A}\sinh\left(\frac{\tau_{eq}}{\tau_0}\right) \tag{10}$$

From these equations it follows that the driving stress response $\mathbf{S}^d$, as described in this model, can be depicted as a single Maxwell mode employing a non-linear relaxation time $\lambda = \eta(\tau_{eq})/G$. In principle, the viscosity in Eq. (5) can also be augmented to include the effects of hydrostatic pressure and intrinsic strain-softening [4], which, however, is not the subject of this research.

In the case of large stress and strain in a uniaxial compression test, the strain rate dependence of stress can be calculated for the basic Leonov model as follows: the hyperbolic sine term accounts for the back-jumps of the flow unit, which are not negligible at low stresses. When the argument of the hyperbolic sine function is large, i.e. when τ_{eq} is high and back jumps are negligible, it can be approximated by an exponential function so that $\sinh(x) \approx 1/2\ \exp(x)$. Using Eq. (9), Eq. (10) can be rewritten for this limiting case as

$$\dot{\gamma}_{eq} = \frac{1}{2A_0}\exp\left(-\frac{\Delta H}{kT}\right) \quad \text{with} \quad \Delta H = \Delta H_0 - V^*\tau_{eq} \tag{11}$$

where ΔH is the height of the energy barrier at applied stress τ_{eq}. Using the relations $\dot{\gamma}_{eq} = \sqrt{3}\dot{\varepsilon}$, and $\tau_{eq} = \sqrt{1/3}\sigma$ valid for uniaxial deformation, cf. Eqs. (6) and (7), the activation volume V^* can be related to the strain dependence of stress via

$$V^* = kT\sqrt{3}\left(\frac{d\sigma}{d\ln\dot{\varepsilon}}\right)^{-1} \text{ valid for uniaxial deformation} \tag{12}$$

where σ is the total true stress in deformation direction and $\dot{\varepsilon}$ is the total strain rate, assuming that after yielding the plastic strain rate approximately equals the total strain rate. Hence, Eq. (12) provides us with a tool for the direct determination of the theoretical activation volume V^* from experimental data obtained in uniaxial deformation.

3. Experimental

3.1. Materials

The materials used in this study can be divided into two sections. First, an assortment of linear amorphous polymers, which at room temperature are far below their glass transition temperatures (at least 80 K), and, which cover a wide range of entanglement densities, cf. Table 1. Second, chemically cross-linked poly(methylmethacrylate) (PMMA) with varying cross-link density. Linear polymers were obtained from Polymer Laboratories, UK, except polystyrene (PS), commercial grade PMMA (PMMAc), polycarbonate (PC) (Aldrich, CH) and poly(2,6-dimethyl-1,4-phenylene oxide) (commercial grade PPO) (PolySciences, USA).

Cross-linking of PMMA (commercial grade, PMMAc) was achieved by 1,10-diaminodecane, where the amidation-reaction was catalyzed by *p*-toluenesulfonic acid [20]. Weighted quantities of polymer, diamine, and catalyst were dissolved in methylene-chloride. Amounts of diamine were chosen such that the final cross-link density were varied from values of the order of the entanglement density ρ_e of the corresponding melt to values of about $10\rho_e$. The catalyst amounted to 2–3% equiv of the amine. After stirring for 5 min, the solution was poured into a petri-dish and the solvent was allowed to evaporate at room temperature over a period of 4 days. To maintain the cross-link reaction effectively, an optimal temperature of 150 °C had been determined empirically. Hence, cross-linked PMMA samples were prepared by keeping the compression temperature of 150 °C in the mold over a period of 4 days before cooling down.

The cross-link density was determined by measuring the elastic modulus in uniaxial compression of samples swollen in *N*,*N*-dimethylformamide, where the volume fraction of the polymer v_2 in the swollen samples was determined by measuring their buoyant force in hexane. Application of the well-known phantom model [21,22], which satisfactorily describes the rubber-elastic response of the swollen network, yields directly the effective average cycle rank ξ per volume from the experimental elastic modulus G:

Table 1
Materials

Material	Notation	M_W	M_W/M_N	T_g (K)	ρ_e (1/nm^3)
Polystyrene	PS96K	96,000	1.03	363	0.0219
	PS483K	483,000	1.05		
	PS1M	1,000,000	1.03		
	PS4M	3,900,000	1.05		
Poly(methylmethacrylate)	PMMA55K	55,600	1.02	388	0.0340
	PMMA100K	100,000	1.04		
	PMMA254K	254,100	1.04		
	PMMA772K	772,000	1.03		
	PMMA1M	1,520,000	1.08		
	PMMAc	120,000	3.00		
Poly(phenyleneoxide)	PPO	50,000	2.50	483	0.1046
Polycarbonate	PC64K	64,000	1.66	418	0.2581

M_W is the weight averaged molecular weight, M_N the number averaged molecular weight, M_W/M_N the polydispersity, T_g the glass transition temperature, and ρ_e the entanglement density in units of entanglements per volume [19].

$$\sigma = G(\alpha^2 - \alpha^{-1}) \quad \text{with} \quad G = \frac{\xi kT}{V_d} v_2^{1/3} \tag{13}$$

Here σ is the true compressive stress, α the isochoric draw ratio, ξ the number of network chains that must be cut to reduce the network to a state containing no closed cycles, V_d the sample volume in the dry state, and kT the thermal energy. Finally, from the knowledge of the cycle rank ξ, the effective average number of cross-links per unit volume μ can be approximated in the limit of many chains [23] by $\mu = \xi(f/2-1)^{-1}$, where f is the effective functionality of the network, which is assumed to be $f=4$.

3.2. Sample preparation

Cylindrical samples (diameter 4mm, height 3mm) were prepared by compression molding at temperatures 30K–50K above the glass transition temperature of the material at a very slow compression rate (<0.5 mm/min). This allowed the material to flow into the hot mold and approach an equilibrium state within a time window of 30 min. In this way, flow induced orientation of the polymer chains were minimized. Subsequently, to minimize temperature gradients in the sample, the temperature was decreased slowly to room temperature (< 0.6 K/min), at a pressure of less than 20 MPa. Degradation was avoided by a careful choice of the compression temperature and sealing of the mold. In a final step, flat parallel top and bottom surfaces were obtained by polishing.

3.3. Methods

All uniaxial compression experiments were performed at constant true strain rate on a mechanical tensile and compression tester Z020 from Zwick GmbH & Co KG, Germany. The sample dimension along the compression direction was derived from the cross-head displacement of the tensile tester and corrected instantly for the finite compliance of the whole test setup before data acquisition. The lateral sample dimension of the cylindrical symmetric samples was measured using a video extensometer from Messphysik Materials Testing, Austria.

Friction between the steel plates of the compression setup and the sample surfaces was minimized by placing a thin sheet of Teflon (0.02 mm thickness) in combination with commercial fluid dishwasher (a 6/1 blend of anionic tensides and soap) between the surface of the sample and the compression plates. In this way bulging were avoided up to the maximum applied strains (of about $\varepsilon = -0.9$).

All experiments were performed at compressive strain rates $|\dot{\varepsilon}| \leq 10^{-2}\ \mathrm{s}^{-1}$ using a sample geometry with a high surface-to-volume ratio of 1.6 to optimize heat transfer with the surrounding. Temperature effects on true stress–strain curves due to internal heat generation have been reported in literature [24,25], but occurring at strain rates $|\dot{\varepsilon}| \geq 3 \times 10^{-2}\ \mathrm{s}^{-1}$ for samples with lower surface to volume ratios (in the range 0.5–1).

4. Results

The focus of this study is on finite large-strain deformation behavior of polymer glasses, with the emphasis on the influence of strain-rate. Note that the terms stress and strain (rate) always refer to true stress and true strain (rate) unless indicated otherwise. Isothermal stress–strain plots have been obtained in uniaxial compression at room temperature from the polymeric glasses listed in Table 1. Each listed material was tested at 4–5 different constant strain rates, to be called a 'set'. In total a number of 35 sets have been obtained experimentally, thus resulting in a reliable number of statistical significant experiments. According to Eq. (12), the yield stress σ_y, usually defined as the local stress maximum, which is considered to mark the onset of plastic flow, is a linear function of logarithmic strain-rate:

$$\frac{d\sigma_y}{d\ln\dot{\varepsilon}} = \frac{\sqrt{3}kT}{V^*} \neq f(\dot{\varepsilon}) \quad \text{at} \quad \varepsilon = \varepsilon_{yield} \tag{14}$$

A good approach to analyze strain-rate effects on stress at large finite deformations might be to verify the linearity of the $\sigma - \ln\dot{\varepsilon}$ relation not only at the yield point, but as a function of strain covering the complete post-yield regime from medium to finite strains. This leads to the more general equation

$$\frac{d\sigma(\varepsilon)}{d\ln\dot{\varepsilon}} = \Gamma(\varepsilon) \neq f(\dot{\varepsilon}) \quad \text{at} \quad \varepsilon \geq \varepsilon_{yield} \tag{15}$$

where $\Gamma(\varepsilon)$ denotes an initially strain-rate independent unknown function of the actual state of deformation presented by the total strain ε. For all sets of compression tests, the stress at a certain fixed strain ε=const. was plotted against the logarithmic strain-rate, and the quadratic correlation coefficient R^2 [26] of a linear fit to the data was determined to evaluate the linearity of the $\sigma(\varepsilon) - \ln\dot{\varepsilon}$ relation as a function of total strain ε, cf. Eq. (15). Fig. 2 shows values of the quadratic correlation coefficient R^2. In this figure it can be seen, that the quality of the linear fit improves with increasing strain, featuring

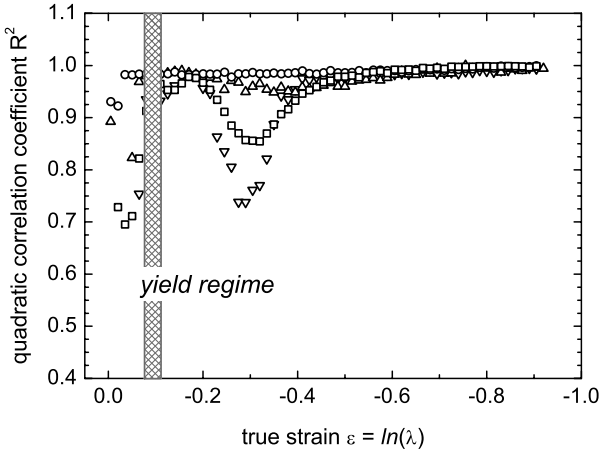

Fig. 2. Correlation coefficient R^2 of a linear fit to $\sigma(\varepsilon) - \ln\dot{\varepsilon}$ plots as a function of true strain according to the data of Figs. 3 and 4. Down triangles: PC64K, up triangles: PS483K, squares: PPOc, circles: PMMA772K. To visualize the post-yield regime, the approximate strain interval, which covers the onset of yield of all four polymers, is indicated by the hatched area.

a quadratic correlation coefficient not falling below 0.85, with exception of the curves for PC, which depict an inferior fit in the strain softening regime around $\varepsilon \approx -0.3$. This is due to the fact, that, in general, the strain-rate dependence of stress–strain plots of PC is relatively small, hence the dependence on strain-rate being much more sensitive to experimental errors. Nevertheless, Fig. 2 indicates, that the stress appears to be a linear function of the logarithmic strain-rate to a good approximation, not only at the yield point, but at any state of deformation in the post yield regime. Note that no model assumption on the strain dependence of $\Gamma(\varepsilon)$ is included in Eq. (15) or can be extracted from Fig. 2.

Figs. 3 and 4 shows representative stress–strain curves of PMMA, PPO, PC, and PS recorded at five different strain-rates in the range $|\dot{\varepsilon}| = 10^{-4}\ \mathrm{s}^{-1}$ to $|\dot{\varepsilon}| = 10^{-2}\ \mathrm{s}^{-1}$. Additionally, the dotted line in every subfigure shows the linear dependence of stress on the logarithmic strain-rate as a function of strain, i.e. the dotted line in each subfigure presents $\Gamma(\varepsilon)$ according to Eq. (15). Obviously there is a clear increase of $\Gamma(\varepsilon)$ with increasing strain in the post-yield regime succeeding the local stress minimum, i.e. succeeding strain-softening. This qualitative effect had been generally observed in uniaxial compression tests for all glassy polymers in this study, independently of degree of cross-linking, molecular weight or polydispersity.

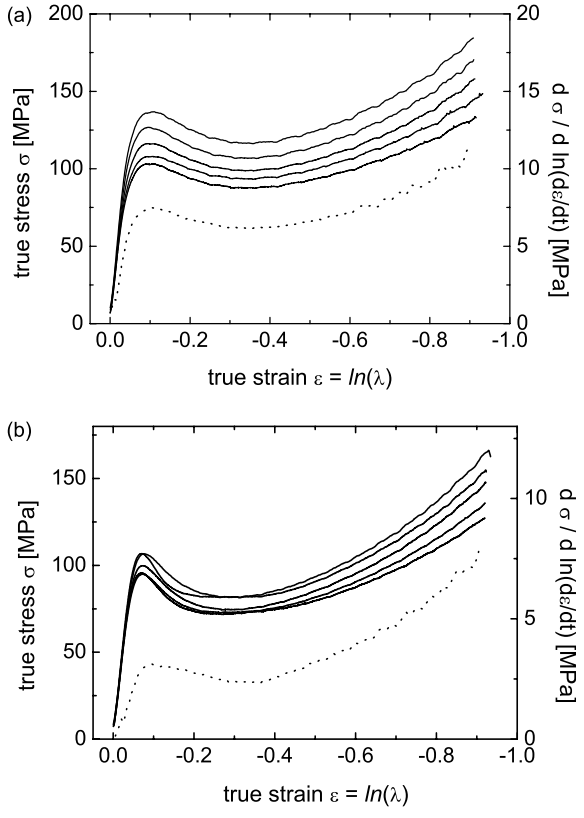

Fig. 3. Solid lines: experimental isothermal stress–strain data obtained at room temperature: (a) PMMA772K, (b) PPO. All curves were obtained in uniaxial compression at constant true strain-rates $|\dot{\varepsilon}|$ increasing from bottom to top ($10^{-4}\ \mathrm{s}^{-1}$, $3\times10^{-4}\ \mathrm{s}^{-1}$, $10^{-3}\ \mathrm{s}^{-1}$, $3\times10^{-3}\ \mathrm{s}^{-1}$, and $10^{-2}\ \mathrm{s}^{-1}$). Dotted lines: derivative of true stress with respect to logarithmic strain-rate $\mathrm{d}\sigma(\varepsilon)/\mathrm{dln}\ \dot{\varepsilon} = \Gamma(\varepsilon)$.

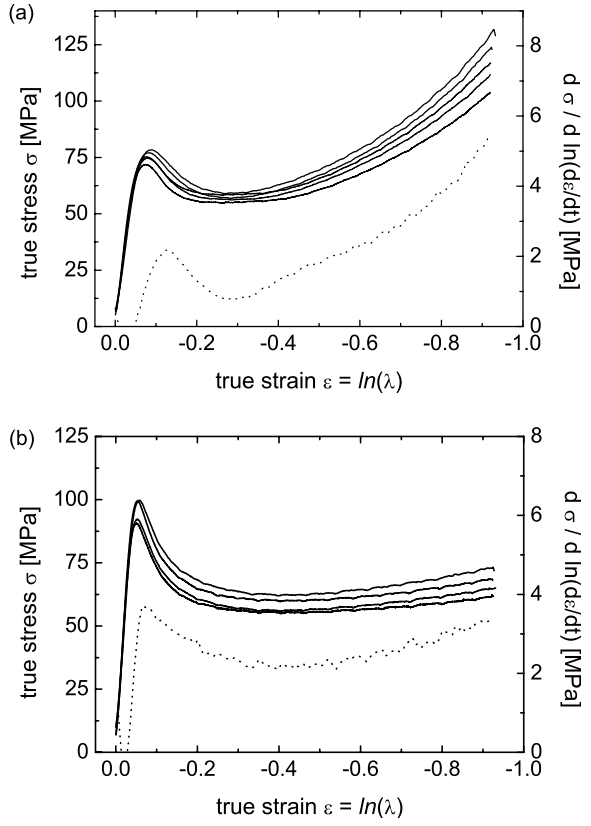

Fig. 4. Solid lines: experimental isothermal stress–strain data obtained at room temperature: (a) PC64K, (a) PS483K. All curves were obtained in uniaxial compression at constant true strain-rates $|\dot{\varepsilon}|$ increasing from bottom to top ($10^{-4}\ \mathrm{s}^{-1}$, $3\times10^{-4}\ \mathrm{s}^{-1}$, $10^{-3}\ \mathrm{s}^{-1}$, $3\times10^{-3}\ \mathrm{s}^{-1}$, and $10^{-2}\ \mathrm{s}^{-1}$ (not for PS483K)). Dotted lines: derivative of true stress with respect to logarithmic strain-rate $\mathrm{d}\sigma(\varepsilon)/\mathrm{dln}\ \dot{\varepsilon} = \Gamma(\varepsilon)$.

Fig. 5 shows the effect of varying cross-link density on engineering stress–strain curves of chemically cross-linked PMMA. For a better visualization of any possible effects, Fig. 5 is presented in engineering units to reduce additional data scattering induced by a further experimental parameter present

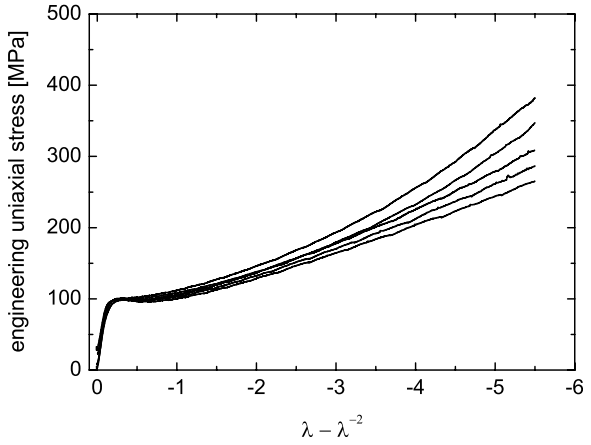

Fig. 5. Engineering uniaxial stress against $\lambda - \lambda^{-2}$ for PMMA with varying cross-link densities increasing from bottom to top: non-cross-linked linear PMMA, $\mu = 0.105$, $\mu = 0.314$, $\mu = 0.627$, $\mu = 0.785$, where μ denotes the absolute average number of effective cross-links per unit volume in units of $(1/\mathrm{nm}^3)$.

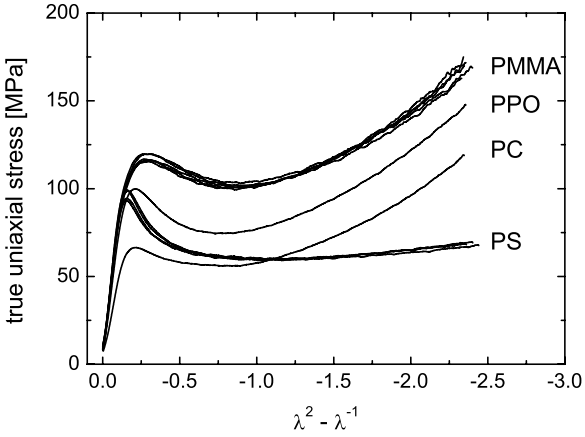

Fig. 6. True uniaxial stress against $\lambda^2-\lambda^{-1}$ for PMMA, PS, PC and PPO recorded at a true strain-rate of $|\dot{\varepsilon}| = 10^{-3}$ s^{-1} with varying (weight averaged) molecular weights M_W for the case of PMMA and PS, according to the materials listed in Table 1. Results for all molecular weights are shown.

in true stress–strain curves, which is the actual area of the sample. Since all samples had the same dimensions and were compressed under identical conditions, engineering units present no constraints with respect to the comparison of the curves. Engineering stress is plotted against $\lambda-\lambda^{-2}$ to visualize any significant deviation from neo-Hookean behavior. From Fig. 5 it can be seen, that increasing cross-link density induces an increasing stress response revealing an increasing deviation from neo-Hookean behavior at large finite deformations. The increasing stress response is normally attributed to an increase of the modulus of the rubber-elastic network response [6], resulting in an increase of stress with increasing network density at large strains, whereas deviation from neo-Hookean behavior is normally attributed to the finite extensibility of the chains [8,27].

However, careful inspection of Fig. 6 appears to indicate that also for the linear non-cross-linked materials a deviation from neo-Hookean behavior can be observed. Note that neo-Hookean behavior manifests itself as a linear dependence of the true stress as a function of λ^2-1/λ.

In addition, Fig. 6 shows that for the case of glassy PMMA and PS, the influence of molecular weight on stress–strain behavior at room temperature is negligible within the scatter of the experiments for the applied range of $300M_e > M_W > 5M_e$, where M_e is the so-called entanglement molecular weight of the corresponding polymer melt.

5. Discussion

In the basic compressible Leonov model, the activation volume V^*, as introduced in Eq. (8), is considered to be an intrinsic material constant. Assuming an elastic neo-Hookean strain-hardening response, such a constant activation volume would always lead to a vertical shift with changing strain-rate of post-yield stress curves as shown in subplots (a) of Figs. 7 and 8. A good test of the validity of this proposition is to plot V^*, obtained from experimental data via Eq. (12), as a function of strain. Interestingly $\Gamma(\varepsilon)$ and therefore also V^*, which is

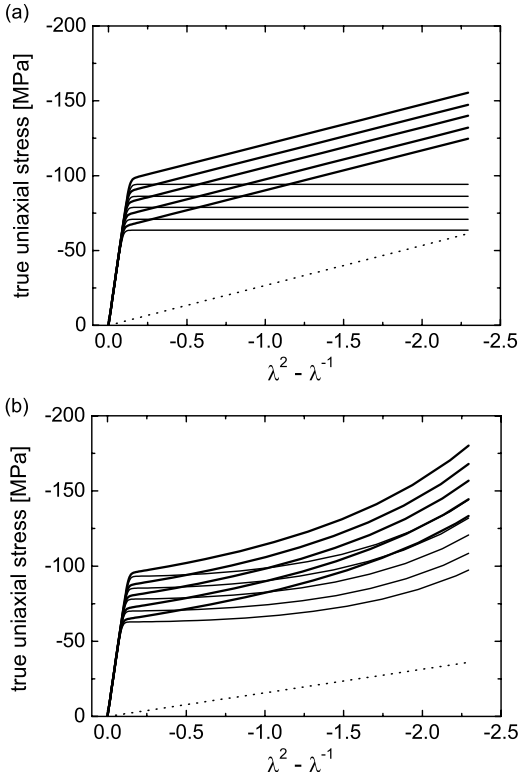

Fig. 7. Simulated true stress–true strain curves in *compression* according to the Leonov model using (a) constant activation volume V^* = constant and (b) non-constant activation volume $V^*(\varepsilon) \propto \sqrt{I_B II_B}$. Parameters for the simulation were chosen from a best fit to experimental compression data of PMMA (cf. Fig. 9). Thin solid lines: viscoelastic response, dashed lines: rubber-elastic response, thick solid lines: total stress response.

inverse proportional to $\Gamma(\varepsilon)$ in uniaxial compression mode like $V^*(\varepsilon) = \Gamma(\varepsilon)^{-1} kT\sqrt{3}$ (cf. Eqs. (12) and (15)), are a function of strain rather than an intrinsic material constant as shown in Figs. 3 and 4 by the dotted lines and already suggested by Pink [18].

The approach presented in the following is a purely empirical relation aimed to get the best agreement between modeling and experimental stress–strain data. In the simplest attempt at visualization, the activation volume V^* might be described as the product of a displacement vector and the area 'swept out' by a plastic event [18]. From kinematics [28] it is known that the extension of a line element in a point P and the change in area of all planes in a point P averaged over all possible orientations are given by the first and second invariants (I_B, II_B) of the isochoric Cauchy–Green strain tensor $\tilde{\mathbf{B}}$, respectively:

$$\left\langle \frac{dl}{l} \right\rangle = \sqrt{\frac{\lambda_1^2+\lambda_3^2+\lambda_3^2}{3}} = \sqrt{\frac{I_B}{3}} \tag{16}$$

$$\left\langle \frac{dA}{A} \right\rangle = \sqrt{\frac{\lambda_1^2\lambda_2^2+\lambda_2^2\lambda_3^2+\lambda_1^2\lambda_3^2}{3}} = \sqrt{\frac{II_B}{3}} \tag{17}$$

Therefore, it is attempted to relate the strain-dependent activation volume $V^*(\varepsilon)$ to the actual state of deformation in

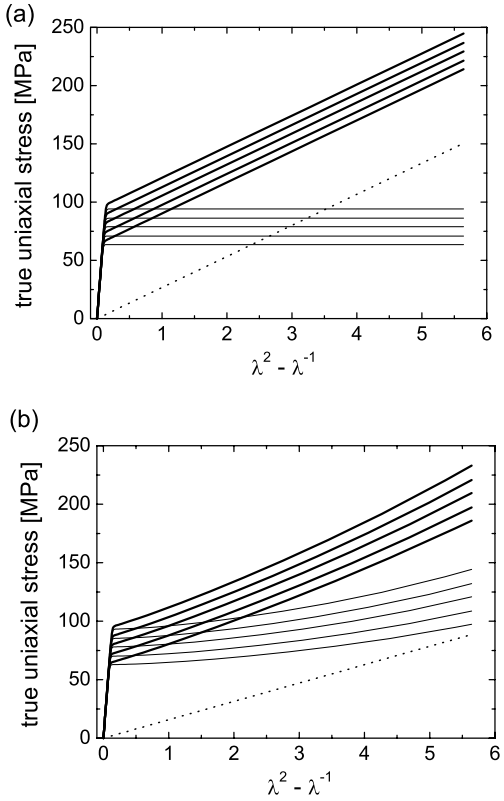

Fig. 8. Simulated true stress–true strain curves in *tension* according to the Leonov model using (a) constant activation volume V^* = constant and (b) non-constant activation volume $V^*(\varepsilon) \propto \sqrt{I_B II_B}$. Parameters for the simulation were chosen from a best fit to experimental compression data of PMMA (cf. Fig. 9). Thin solid lines: viscoelastic response, dashed lines: rubber-elastic response, thick solid lines: total stress response.

the following way:

$$V^* \propto \frac{\sqrt{I_B II_B}}{3} \tag{18}$$

This relation implies, that, at any given fixed strain, $\sigma(\varepsilon) \propto \ln \dot{\varepsilon}$, i.e. that Eq. (15) holds as supported by Fig. 2. Changing the actual state of deformation, i.e. varying the total strain, however, will now change the activation volume according to Eq. (18). Hence, the actual activation volume $V^*(\varepsilon)$ is altered by the total strain through a dependence of the activation volume on invariants of the isochoric Cauchy–Green strain tensor $\tilde{\mathbf{B}}$. For a uniaxial deformation test, assuming incompressibility, the isochoric Cauchy–Green strain tensor $\tilde{\mathbf{B}}$ equals

$$\tilde{\mathbf{B}} = \begin{pmatrix} e^{-\varepsilon} & 0 & 0 \\ 0 & e^{-\varepsilon} & 0 \\ 0 & 0 & e^{2\varepsilon} \end{pmatrix} \tag{19}$$

Using Eq. (19) in Eq. (18) yields

$$V^*(\varepsilon) = \alpha_V - \beta_V \sqrt{(2e^{-\varepsilon} + e^{2\varepsilon})(e^{-2\varepsilon} + 2e^{\varepsilon})} \tag{20}$$

where α_V and β_V are fitting parameters denoting the intercept and slope of the linear relation suggested in Eq. (18).

To demonstrate the effect of this non-constant activation volume on the large strain behavior of the suggested continuum model, subplots (b) of Figs. 7 and 8 show simulated data according to the modified Leonov model using a non-constant activation volume. Here, the parameters for the simulation in compression and tension where chosen to yield a best fit to the experimental large strain compression data of PMMA as shown in Fig. 9. From these plots it can be seen that the introduction of a non-constant activation volume into the viscoelastic response of the compressible Leonov model in combination with an elastic neo-Hookean strain-hardening response generates a strain-rate dependent strain-hardening and upswing of stress at large strains, respectively. In other words, total stress–strain curves obtained at different strain-rates are not parallel at large strains as the in the case of a constant activation volume according to Eqs. (14) and (15) and deviate from neo-Hookean behavior. Note that simulated data in compression and tension were generated with identical parameters whilst the stress upswing at large strains is much less pronounced in tension.

5.1. Linear glassy polymers

Figs. 9(a)–12(a) show representative plots of PMMA, PPO,

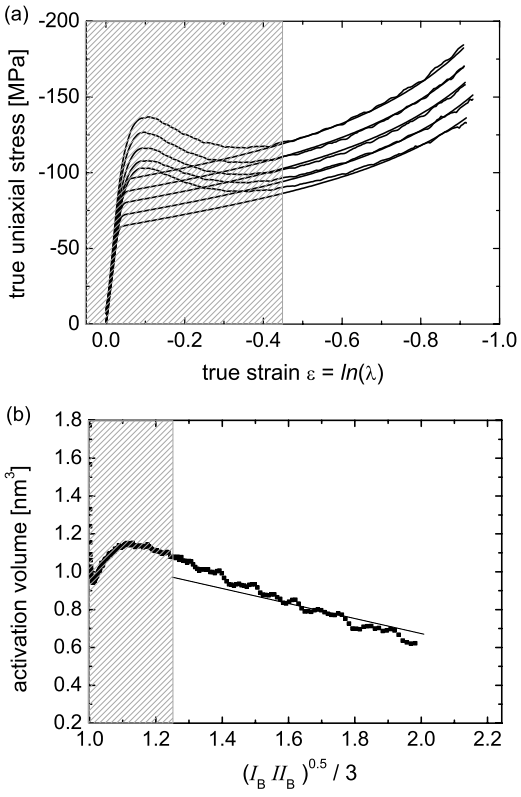

Fig. 9. (a) True stress–true strain plot of PMMA772K obtained in uniaxial compression at different true strain rates $|\dot{\varepsilon}|$ increasing from bottom to top ($10^{-4}\,s^{-1}$, $3\times10^{-4}\,s^{-1}$, $10^{-3}\,s^{-1}$, $3\times10^{-3}\,s^{-1}$, and $10^{-2}\,s^{-1}$). (b) Experimental activation volume determined via Eq. (12) from the plots in (a) as a function of $\sqrt{I_B II_B}/3$, as suggested in Eq. (18). Solid lines show the best fit of continuum model simulations with a non-constant activation volume to the experimental data in the non-hatched region of the graph.

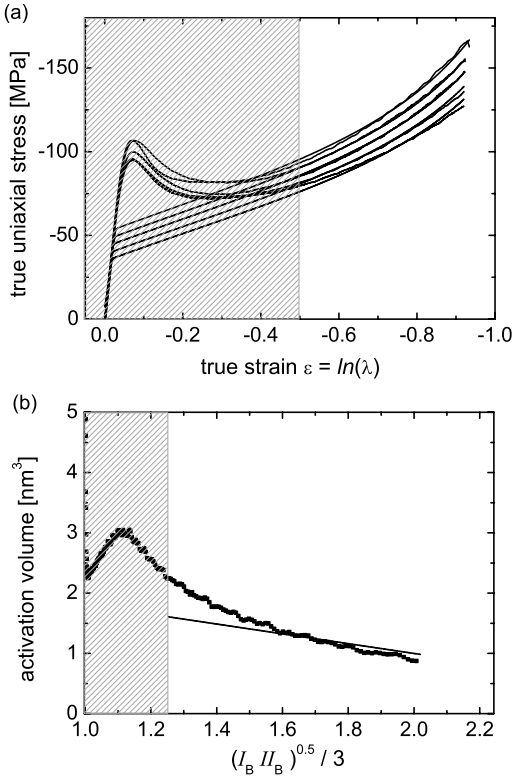

Fig. 10. (a) True stress–true strain plot of PPOc obtained in uniaxial compression at different true strain rates $|\dot{\varepsilon}|$ increasing from bottom to top ($10^{-4}\,s^{-1}$, $3\times10^{-4}\,s^{-1}$, $10^{-3}\,s^{-1}$, $3\times10^{-3}\,s^{-1}$, and $10^{-2}\,s^{-1}$). (b) Experimental activation volume determined via Eq. (12) from the plots in (a) as a function of $\sqrt{I_B II_B}/3$, as suggested in Eq. (18). Solid lines show the best fit of continuum model simulations with a non-constant activation volume to the experimental data in the non-hatched region of the graph.

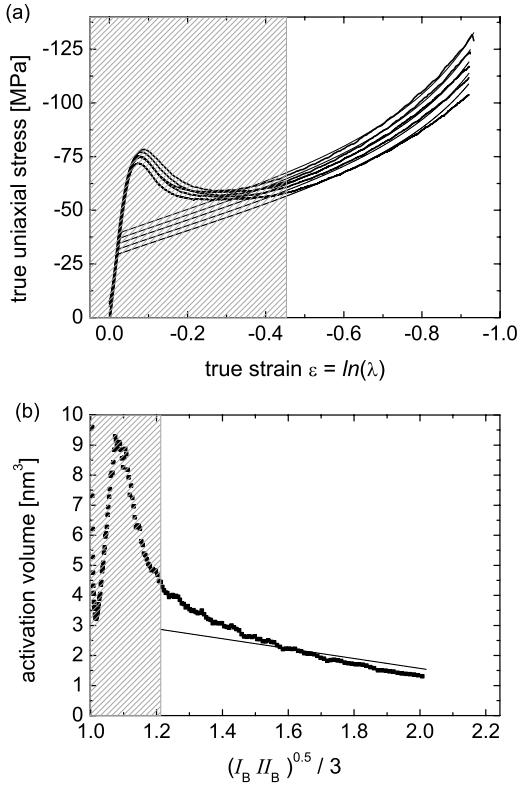

Fig. 11. (a) True stress–true strain plot of PC64K obtained in uniaxial compression at different true strain rates $|\dot{\varepsilon}|$ increasing from bottom to top ($10^{-4}\,s^{-1}$, $3\times10^{-4}\,s^{-1}$, $10^{-3}\,s^{-1}$, $3\times10^{-3}\,s^{-1}$, and $10^{-2}\,s^{-1}$). (b) Experimental activation volume determined via Eq. (12) from the plots in (a) as a function of $\sqrt{I_B II_B}/3$, as suggested in Eq. (18). Solid lines show the best fit of continuum model simulations with a non-constant activation volume to the experimental data in the non-hatched region of the graph.

PC, and PS together with least squares fits (thin solid lines) of the suggested modified Leonov model including a non-constant activation volume according to Eq. (18). Fitting parameters were G, A, α_V, β_V, and G_R, cf. Tables 2 and 3.

Figs. 9(b)–12(b) show the experimental activation volume determined from stress–strain plots via Eq. (12) together with the activation volume $V^*(\varepsilon)$ (solid lines) according to the suggested model. Note that the solid lines do not show a fit of Eq. (20) to the experimental activation volume. Instead, $V^*(\varepsilon)$ was calculated with fitting parameters α_V and β_V, cf. Eq. (20) and Table 2, which were obtained from a least squares fit of the model to stress–strain data as shown in Figs. 9(a)–12(a).

The aim of this study is to investigate plastic deformation of glassy polymers at large finite strains. As shown by numerous authors [4,11,29,30], strain softening has no influence on the large strain behavior of polymer glasses. Hence, fitting of the experimental stress–strain curves with the modified Leonov model was always chosen to start after the local strain softening minimum and the hatched areas of the graphs were not taken into account, except for the initial elastic modulus of the calculated curves, which was determined from the experimental stress–strain curves at small strain. In this way, fitting the experimental large strain data results in a constitutive model for the fully rejuvenated material. To obtain a correct description of the initial yield stress and subsequent yield drop, the rejuvenated stress–strain response would need to be corrected for the increase in yield stress due to physical aging and the subsequent strain-softening upon plastic deformation [4].

The most obvious feature of these plots is, that the experimental activation volume is not independent of the actual state of deformation, but rather decreases with increasing strain thus, leading to an increasing strain-hardening response with increasing strain-rate. Obviously a good fit of theoretical stress–strain curves to experimental data, cf. Figs. 9(a)–12(a), does not imply that also the experimental activation volume is described by the model to the same level of accuracy. This is due to the fact that $V^*(\varepsilon)$ is inverse proportional to $d\sigma/d\ln\dot{\varepsilon}$. Thus, especially in the case of a weak dependence of stress on strain-rate, even small relative deviations between theory and experiment in stress–strain plots, cf. Figs. 9(a)–12(a), can cause larger discrepancies in the theoretical description of the strain dependence of the activation volume, cf. Figs. 9(b)–12(b). Hence, considering both, the stress–strain plots and the strain dependence of the activation volume improves the reliability of the validation of any suggested model. However, in this study it appears that a quantitative description of the experimental strain dependence of stress and activation volume at large deformations can be achieved satisfactorily by the incorporation of a non-constant activation

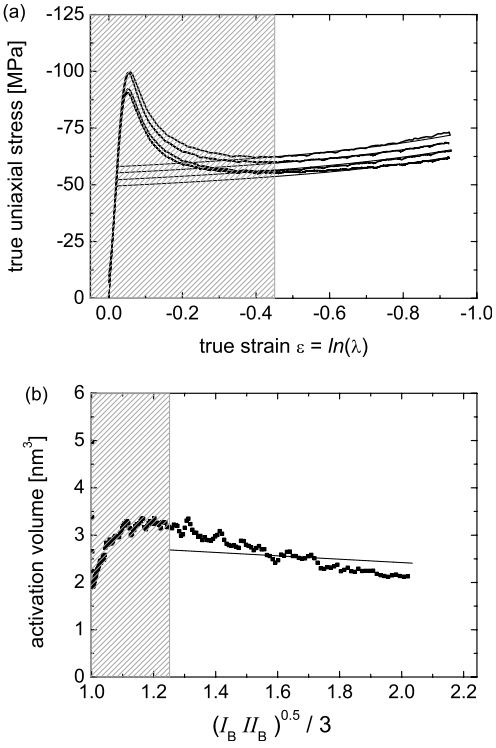

Fig. 12. (a) True stress–true strain plot of PS483K obtained in uniaxial compression at different true strain rates $|\dot{\varepsilon}|$ increasing from bottom to top ($10^{-4}\,s^{-1}$, $3\times10^{-4}\,s^{-1}$, $10^{-3}\,s^{-1}$, $3\times10^{-3}\,s^{-1}$, and $10^{-2}\,s^{-1}$). (b) Experimental activation volume determined via Eq. (12) from the plots in (a) as a function of $\sqrt{I_B II_B}/3$, as suggested in Eq. (18). Solid lines show the best fit of continuum model simulations with a non-constant activation volume to the experimental data in the non-hatched region of the graph.

volume $V^*(\varepsilon)$ in the compressible Leonov model as suggested by Eq. (18).

Again, it should be stressed that in all measurements presented in this paper, a good description of the strain-hardening response using a non-constant activation volume was only obtained by including a neo-Hookean elastic component. Attempts to fit the stress–strain curves solely with a viscous contribution employing a non-constant activation volume were not successful. The physical meaning of a strain-dependent activation volume is not a priori clear. Although the applied fitting relation Eq. (20) is purely phenomenological, its ability to describe the post yield stress–strain behavior so well could indicate that segmental motion is affected not only by stress, but also by orientation of the macromolecular chains as presented by the strain dependence of the activation volume.

Table 2
Fit parameters obtained from a least squares fit of the modified compressible Leonov model to experimental stress–strain data as shown in subplots (a) of Figs. 9–12

Material	G (MPa)	$A/10^{10}$ (s)	α_V (nm^3)	β_V (nm^3)
PMMA	700	0.0040	1.47	0.40
PPO	446	0.0119	2.72	0.69
PC	490	1.0365	5.75	1.97
PS	750	1523	3.13	0.36

Table 3
Strain–hardening modulus G_R determined by the average slope $d\sigma/d(\lambda^2-\lambda^{-1})$ in the strain interval $-1.5<(\lambda^2-\lambda^{-1})<-2.0$ of Fig. 6, and by a best fit of the modified compressible Leonov model as shown in Figs. 9–12

Material	$G_R = d\sigma/d(\lambda^2-\lambda^{-1})$ (MPa)	G_R by modified comp. Leonov model (MPa)
PMMA	53	23
PPO	55	41
PC	47	31
PS	9	0.7

As noted before, due to application of a non-constant activation volume $V^*(\varepsilon)$, the contribution of the elastic (neo-Hookean) network response to the total strain-hardening is reduced. Therefore, the lower strain-hardening modulus translates into entanglement densities that are lower than in the case of a constant activation volume. Table 3 shows strain-hardening moduli determined from the slopes of Fig. 6 and determined by a best fit of the modified compressible Leonov model to the experimental data in Figs. 9–12. Here, it can be seen, that the contribution of the rubber-elastic network to the strain hardening decreases significantly by the application of a non-constant activation volume. Note, that the value of G_R should not be taken too literally, since it depends on the suggested relation of the activation volume V^* on strain, cf. Eq. (18). The validity of the concept of a network active during plastic deformation in glassy polymers as a generator for strain-hardening and especially segmental orientation is supported by solid-state NMR studies on segmental orientational order in deformed poly(bisphenol A carbonate) [31] and poly(methylmethacrylate) [32,33]. This network is of considerably higher density than the entanglement network.

5.2. Cross-linked PMMA

Best fits of the stress–strain behavior of cross-linked PMMA using the modified Leonov model are shown in Figs. 13 and 14. Interestingly, the function $\Gamma(\varepsilon)$, describing the experimental activation volume as a function of strain, was found to dependent on crosslink density, as depicted in Fig. 15, suggesting the following extension of Eq. (18):

$$V^*(\varepsilon) \propto \mu\sqrt{I_B II_B} \tag{21}$$

where μ is the total average number of cross-links per unit volume. Apparently, a non-constant activation volume is able to describe the increased strain-rate dependent upswing observed for cross-linked glassy PMMA. At the same time the neo-Hookean response is kept more or less constant($\approx 23 \pm 7$ MPa), despite cross-link densities that differ by a factor of seven. Note that there is no need to introduce finite extensibility of network chains to account for the stress upswing at large strains. In this approach, surprisingly, the increased strain-hardening upon cross-linking is due to

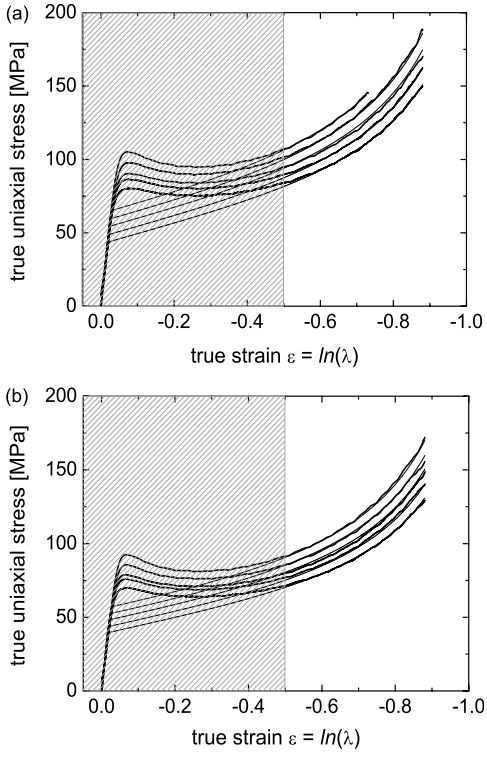

Fig. 13. True stress–true strain plots of cross-linked PMMA with varying cross-link densities μ, (a) 0.785/nm^3, (b) 0.627/nm^3, obtained in uniaxial compression at different true strain rates $|\dot{\varepsilon}|$ increasing from bottom to top curve (10^{-4} s^{-1}, 3×10^{-4} s^{-1}, 10^{-3} s^{-1}, 3×10^{-3} s^{-1}, and 10^{-2} s^{-1}). Thin solid lines show the best fit of continuum model simulations with a non-constant activation volume to the experimental data in the non-hatched region of the graph.

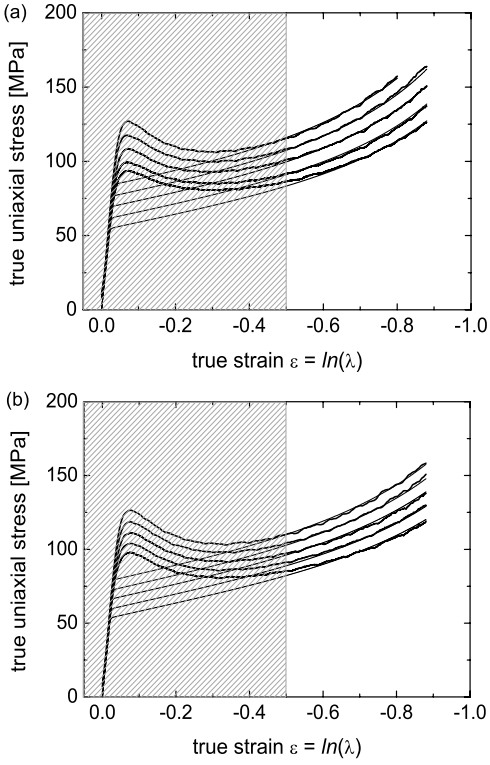

Fig. 14. True stress–true strain plots of cross-linked PMMA with varying cross-link densities μ, (a) 0.314/nm^3, and (b) 0.105/nm^3, obtained in uniaxial compression at different true strain rates $|\dot{\varepsilon}|$ increasing from bottom to top curve (10^{-4} s^{-1}, 3×10^{-4} s^{-1}, 10^{-3} s^{-1}, 3×10^{-3} s^{-1}, and 10^{-2} s^{-1}). Thin solid lines show the best fit of continuum model simulations with a non-constant activation volume to the experimental data in the non-hatched region of the graph.

the modification of the activation volume rather than an increased elastic neo-Hookean contribution. The independence of the strain hardening modulus on cross-link density, as suggested in this study, may be counter-intuitive since cross-linking clearly increases the rubber-elastic modulus above T_g. However, there is a large discrepancy between the strain-hardening modulus measured at room temperature and the rubber-elastic modulus above T_g, as was also noticed by others [6,11]. As a result, entanglement densities calculated from the high strain-hardening moduli measured at room temperature tend to be extremely high, much higher than common values for entanglement and cross-link densities observed above T_g. It is, therefore, not clear whether there should be a direct correlation between the rubber-elastic response of an entangled or cross-linked network above T_g and a neo-Hookean strain-hardening response below T_g, except possibly at very high entanglement or network densities, such as in the case of poly(carbonate) [34]. However, the chemical cross-link density, as shown in this study, as well as the entanglement density of linear glassy polymers, as shown recently by Ho et al. [35], seem to affect the viscous part of the total stress significantly, which can be accounted for by using a strain and crosslink-dependent activation volume. The importance of thermal mobility of polymer chains on strain-hardening was also recognized by van Melick et al. [6].

In other words, the network density of linear and cross-linked PMMA calculated from the strain-hardening modulus at room temperature is much higher than the entanglement or chemical cross-link densities applied in this study, which could explain the relative insensitivity of the strain-hardening

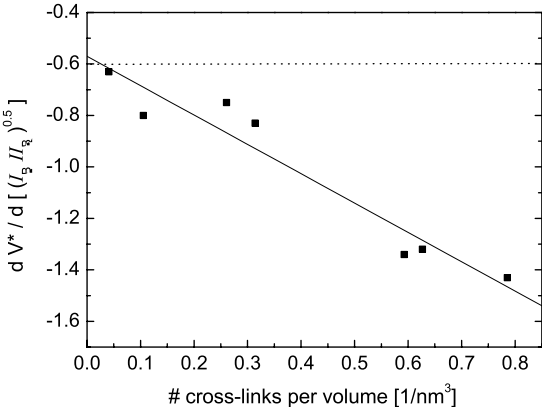

Fig. 15. Change of the activation volume with increasing cross-link density for chemically cross-linked PMMA according to the suggested dependencies of Eq. (18) on invariants of the Cauchy–Green strain tensor. The dotted lines indicate the corresponding value for the non-cross-linked material. The solid line presents a linear fit to the data suggesting a linear dependence of the activation volume on the cross-link density as described in Eq. (21).

modulus to cross-link density. Note that the mentioned insensitivity is a consequence of the suggested model using a strain dependent activation volume. Moreover, this insensitivity has also been supported by NMR experiments [33], which show that the average orientational distribution of polymer chain segments in plastically deformed glassy PMMA is independent of cross-link density. This suggests that the same rubber-elastic network response as found in this study is also the generator for segmental orientation in the glassy state, insensitive to the applied cross-link densities.

6. Conclusions

In this paper, the compressible Leonov model augmented with an elastic neo-Hookean network response is modified by a non-constant activation volume to describe the strain-rate dependence of the strain-hardening and the stress-upswing at large compressive strains of polymer glasses, in good agreement with experimental data. However, validation of the suggested model for loading geometries different from uniaxial compression has not yet been explored.

The activation volume could be described as an empirical function of invariants of the left Cauchy–Green strain tensor or the equivalent stress tensor of the network. According to this approach, the rate-dependent upswing of stress, observed in linear and cross-linked glassy systems in this study, is not related to the finite extensibility of network chains, but rather to a change in the viscoelastic response.

For the chemically cross-linked materials, within the range of cross-link densities applied in this study, the neo-Hookean part of the strain-hardening response was found to be independent of chemical cross-link density. It was found that the increase in the total strain-hardening response upon cross-linking could be described by a change in the viscoelastic response, expressed by a dependence of the activation volume on strain and cross-link density.

A Matlab package ‘Leonov’ for the implementation of the modified Leonov model as suggested in this study is available free of charge via the Internet at http://www.mathworks.com/matlabcentral/fileexchange/.

Acknowledgements

This study has been supported in part by the Swiss National Science Foundation.

References

[1] Ward IM. Mechanical properties of solid polymers. Chichester: Wiley; 1993.
[2] Hodge IM. Physical aging in polymer glasses. Science 1995;267(5206): 1945.
[3] Ward IM. Mechanical properties of solid poylmers. Chichester: Wiley; 2004.
[4] Govaert LE, Timmermans PHM, Brekelmans WAM. The influence of intrinsic strain softening on strain localization in polycarbonate: modeling and experimental validation. J Eng Mater Technol-Trans ASME 2000; 122(2):177.
[5] Hasan OA, Boyce MC, Li XS, Berko S. An investigation of the yield and post-yield behavior and corresponding structure of poly(methyl methacrylate). J Polym Sci, Part B: Polym Phys 1993;31(2):185.
[6] van Melick HGH, Govaert LE, Meijer HEH. On the origin of strain hardening in glassy polymers. Polymer 2003;44:2493.
[7] Haward RN, Thackray G. Use of a mathematical model to describe isothermal stress–strain curves in glassy thermoplastics. Proc R Soc London, Ser A-Math Phys Sci 1968;302(1471):453.
[8] Boyce MC, Parks DM, Argon AS. Large inelastic deformation of glassy-polymers. 1. Rate dependent constitutive model. Mech Mater 1988;7(1):15.
[9] Haward RN. The application of a simplified model for the stress–strain curves of polymers. Polymer 1987;28(9):1485.
[10] Haward RN. Strain-hardening of thermoplastics. Macromolecules 1993; 26(22):5860.
[11] Tervoort TA, Govaert LE. Strain-hardening behavior of polycarbonate in the glassy state. J Rheol 2000;44(6):1263.
[12] van Melick HGH, Govaert LE, Meijer HEH. Prediction of brittle-to-ductile transitions in polystyrene. Polymer 2003;44(2):457.
[13] van Melick HGH, Govaert LE, Meijer HEH. Localisation phenomena in glassy polymers: influence of thermal and mechanical history. Polymer 2003;44(12):3579.
[14] Meijer HEH, Govaert LE. Multi-scale analysis of mechanical properties of amorphous polymer systems. Macromol Chem Phys 2003;204(2):274.
[15] Tervoort TA, Klompen ETJ, Govaert LE. A multi-mode approach to finite, three-dimensional, nonlinear viscoelastic behavior of polymer glasses. J Rheol 1996;40(5):779.
[16] Eyring H. Viscosity, plasticity, and diffusion as examples of absolute reaction rates. J Chem Phys 1936;4:283.
[17] Pink E. Structural variations affecting eyring analysis of macro deformation in polymers. Mater Sci Eng 1976;22(1):85.
[18] Pink E. Applications of the eyring rate theory to the macro deformation of glassy polymers. Reviews on the deformation behavior of materials. vol. 2. Tel Aviv: Freund; 1977 p. 37.
[19] Fetters LJ, Lohse DJ, Richter D, Witten TA, Zirkel A. Connection between polymer molecular-weight, density, chain dimensions, and melt viscoelastic properties. Macromolecules 1994;27(17):4639.
[20] Erman B, Wagner W, Flory PJ. Elastic-modulus and degree of cross-linking of poly(ethyl acrylate) networks. Macromolecules 1980;13(6): 1554.
[21] Flory PJ. Statistical thermodynamics of random networks. Proc R Soc London, Ser A-Math Phys Eng Sci 1976;351(1666):351.
[22] Erman B, Mark JE. Structures and properties of rubberlike networks. Topics in polymer science. Oxford: Oxford University Press; 1997.
[23] Pearson DS, Graessley WW. Structure of rubber networks with multifunctional junctions. Macromolecules 1978;11(3):528.
[24] Arruda EM, Boyce MC, Jayachandran R. Effects of strain-rate, temperature and thermomechanical coupling on the finite strain deformation of glassy-polymers. Mech Mater 1995;19(2–3):193.
[25] Baselmans H. A new modelling approach of rate dependent softening in glassy polymers. Master Thesis, MT 02.11. Eindhoven University of Technology; 2002.
[26] Edwards AL. The correlation coefficient. An introduction to linear regression and correlation. San Francisco, CA: W.H. Freeman; 1976 p. 33.
[27] Wu PD, van der Giessen E. On improved network models for rubber elasticity and their applications to orientation hardening in glassy-polymers. J Mech Phys Solids 1993;41(3):427.
[28] Macosko CW. Rheology: principles, measurements, and applications. New York: VCH; 1994 [chapter 1].
[29] Hasan OA, Boyce MC. Energy-storage during inelastic deformation of glassy-polymers. Polymer 1993;34(24):5085.

[30] Hasan OA, Boyce MC. A constitutive model for the nonlinear viscoelastic viscoplastic behavior of glassy-polymers. Polym Eng Sci 1995;35(4):331.
[31] Utz M, Atallah AS, Robyr P, Widmann AH, Ernst RR, Suter UW. Solid-state NMR investigation of the structural consequences of plastic deformation in polycarbonate. 1. global orientational order. Macromolecules 1999;32(19):6191.
[32] Wendlandt M. Finite deformation of polymeric glasses: continuum modelling and molecular orientation. PhD Thesis, No. 15077. ETH Zurich, Switzerland; 2003.
[33] Wendlandt M, Tervoort TA, Van Beek JD, Suter UW. Segmental orientation in plastically deformed glassy PMMA. Submitted for publication.
[34] Govaert LE, Tervoort TA. Strain hardening of polycarbonate in the glassy state: influence of temperature and molecular weight. J Polym Sci, Part B: Polym Phys 2004;42(11):2041.
[35] Ho J, Govaert L, Utz M. Plastic deformation of glassy polymers: correlation between shear activation volume and entanglement density. Macromolecules 2003;36(19):7398.